IRSTI 31.15.13 https://doi.org/10.26577/phst20251222

Highly efficient copper–palladium nanoalloy catalysts on modified carbon supports

M.K. Skakov[1], A. Amirov[2*], A.K. Kabdrakhmanova[2, 3, 4], N. Toshkuvatova[5], A.T. Khalmanov[6], A.Zh. Miniyazov[1], V.V. Baklanov[1], Y.T. Koyanbayev[1], N.M. Mukhamedova[1], G.K. Zhanbolatova[1], K. Pramod[7] and A. Shakeel[8, 9]

[1]Institute of Atomic Energy, Branch RSE NNC RK, Kurchatov, Kazakhstan
[2]Satbayev University, Almaty, Kazakhstan
[3]Scientific Research Institute "TrueScience", Almaty, Kazakhstan
[4]LLP "SciCom", Astana, Kazakhstan
[5]Samarkand State University named after Sh. Rashidov, Samarkand, Uzbekistan
[6]Samarkand State University of Architecture and Construction named after Mirzo Ulugbek, Samarkand, Uzbekistan
[7]School of Nanoscience and Nanotechnology, Mahatma Gandhi University, Kottayam, India
[8]Postgraduate Department of Chemistry, Government Postgraduate College Rajouri, Jammu and Kashmir, India
[9]Higher Education Department, Government of Jammu and Kashmir, Jammu, India
*e-mail: alseit.amirov@gmail.com

(Received September 22, 2025; received in revised form November 13, 2025; accepted November 19, 2025)

Catalytic systems were made using Cu, Pd, and Pd-Cu nanoparticles (NPs) supported on modified activated carbon (ACm) of BAU-A grade, which had been modified with hydrochloric acid, for dehydrochlorination of chlorobenzene and 1,2-dichlorobenzene. Based on previous studies, the optimal content of metal NPs in the heterogeneous catalysts for the transformation of mono- and dichlorobenzene organochlorine pollutants utilizing the method of catalytic dehydrochlorination were determined to be: 5% for Pd; 10% for Cu; and, 3% Pd and 7% Cu for the bimetallic variant. The metal NPs were determined to bond to the carboxyl and carbonyl functional groups of the ACm. The characteristics of the catalysts were studied using FTIR spectroscopy, differential thermogravimetric analysis, scanning electron microscopy and ad-sorption porosimetry. Finally, following dehydrochlorination, a chromatograph mass spectrometer was used to identify the products. These results on the pore structures of the catalysts demonstrate good development, allowing for an increased number of sites to adsorb persistent organic pollutants (POPs). Whereas all the catalysts showed effectiveness in dehydrochlorination of chlorobenzene and 1,2-dichlorobenzene, separately, into benzene, the bimetallic catalyst, 3Pd-7Cu/ACm, demonstrates the best results, with conversion rates of 93.94% and 89.79%, respectively.

Keywords: hydrodechlorination, copper nanoparticles, palladium nanoparticles (NPs), catalysis, bimetallic catalyst, organochlorine compounds, modified carbon, persistent organic pollutants (POPs).
PACS number(s): 82.65.+r, 68.43.–h, 81.05.U–, 82.20.–w, 81.07.–b.

1. Introduction

Halogen-containing organic compounds are extensively utilized in various industries and by consumers, serving as coolants, medicines and their delivery systems, solvents, and plasticizers, and many other applications. Due to their high toxicity and chemical stability, numerous halogenated organic compounds are identified as persistent organic pollutants (POPs). Consequently, many of these compounds are banned by the World Health Organization (WHO). On May 22, 2001, the Stockholm Convention on Persistent Organic Pollutants was signed. This agreement aims to reduce and eventually eliminate existing stocks of POPs, as well as to cease the production, use, and release of any new POPs [1]. The currently accumulated reserves of excessively produced halogen-containing by-products require environmentally safe handling. This necessitates the development of new methods for their conversion and disposal. Modern methods

of neutralizing waste containing POPs utilize reductive dechlorination. This process can be optimized to save more re-sources by using new types of nanocaalysts that regenerate the hydrocarbon component of halogenated molecules [2].

The development of reductive methods for the dechlorination of organohalogen compounds is facilitated by the search for active, selective, and efficient catalysts. Several studies have demonstrated that catalysts based on palladium (Pd) and platinum (Pt) exhibit the highest activity and selectivity in the reductive transformation of chlorine-containing compounds [3-7]. This is attributed to their capacity to facilitate the separation of H_2, thereby promoting the cleavage of the C–Cl bond [8]. Many studies have been devoted to the analysis of catalysts based on Pd and Pt for the electrocatalytic reduction of halogenated, specifically chlorine-containing, organic compounds. Typically, the content of Pd and Pt in such catalysts reaches 10% by weight [9-12]. However, the utilization of noble metals increases the cost of catalysts and thus, the entire process. In recent years, there has been a trend to alleviate the cost of catalysts by diluting or substituting these expensive noble metals with others that are more economical yet still exhibit acceptable characteristics.

Carbon carriers are highly promising for catalytic applications due to their purity, exceptional porous structure, and high specific surface area [13]. Activated carbon (AC), in particular, is extensively utilized as a carrier material in the synthesis of catalysts aimed at recycling persistent organic pollutants (POPs) [14-17]. Granular activated carbon (GAC) combined with bimetallic Pd and Fe nanoparticles (NPs) was used for the simultaneous adsorption and dehalogenation of polychlorinated biphenyl (PCB) [17]. For this purpose, the pore volume of granular activated carbon is impregnated with a solution of Fe (III) nitrate Fe(NO3)3, followed by heat treatment at a temperature of 3000C. Subsequent reduction with sodium borohydride (NaBH4) leads to the formation of zerovalent (ZVI) Fe0, with Fe NPs sizes in the range of 7-40 nm. Afterwards, the reduced Pd solution (Pd(CH3CO2)2 is added to the surface of Fe NPs. As a result, small stable Fe NPs of 6-12 nm in size are formed in the mesopores of the granular AC, on which a 2-3 nm Pd nanolayer has been uniformly dis-tributed. The GAC/ZVI/Pd system demonstrated 90% efficiency in the dechlorination of 2-chlorobiphenyl to form the reaction product biphenyl. In previous studies, the hydrodechlorination of organohalogen substances with Pd catalysts supported on coal-based material was 80-100% [18-22]. Some researchers developed na-nosized palladium catalysts for the reductive dechlorination of PCBs, achieving this at low temperatures and with a minimal amount of catalyst [23-26]. Fifteen PCB congeners, including monochlorinated (PCB 1, PCB 2), dichlorinated (PCB 4, PCB 5, PCB 7, PCB 9, PCB 10, PCB 11, PCB 12, PCB 14, PCB 15), trichlorinated (PCB 29), tetrachlorinated (PCB 77), pentachlorinated (PCB 126), and hexachlorinated (PCB 169), under-went complete decomposition. This process resulted in a 100% yield of biphenyl using 10% Pd/C–Et3N as a catalyst [27]. In this case, the reductive dechlorination of PCBs was carried out at room temperature in MeOH, with bottled hydrogen as a reducing agent, Pd (10%)/C, and Et3N. 2.5 mg of catalyst was consumed per 25 mg of PCB.

Despite the high catalytic activity of palladium, the high cost of noble metals limits the large-scale production of these catalysts. Recently, copper nanoparticles (Cu NPs) have garnered significant interest in the devel-opment of new catalytic systems due to their high activity and selectivity [28, 33-35]. A study on copper catalysts, with metal contents ranging from 0.5% to 5.0% (wt.), demonstrated the significant impact of the carrier material on alachlor conversion, achieving conversion rates ranging from 85.2% to 92.9% [34]. A catalytic system utilizing copper nanoparticles (Cu NPs) stabilized with polyvinylpyrrolidone (PVPD40) and deposited onto an activated carbon (AC) substrate achieved a chlorobenzene conversion rate of 94.46% [14].

Considering that Cu catalysts for hydrodechlorination have very often been used in conjunction with noble metals, the high conversion rate of alachlor hydrodechlorination is an interesting result from the point of view of scaling [29-32].

Compared to previously reported Pd–Cu catalytic systems, the novelty of this work lies in the use of a Cu-rich composition, which makes it possible to significantly reduce the amount of expensive noble metal without loss of catalytic efficiency. Additionally, the application of HCl-modified wood-based activated carbon as a support is an important distinguishing factor, since chemical modification increases the number of oxygen-containing functional groups and improves the interaction of the metal nanoparticles with the surface, which can promote the formation of more homogeneous and stable Pd–Cu nanoalloys. These two factors together – optimized Pd/Cu ratios and targeted chemical modification of the carbon carrier – create conditions for enhanced Pd–Cu synergy and demonstrate that high hydrodechlorination efficiency can be achieved not only by increasing

Pd loading, but also by engineering the support and nanoalloy composition.

This study focuses on the synthesis and investigation of the physical and chemical properties of Cu, Pd, and Pd-Cu catalysts to evaluate their effectiveness in the liquid-phase hydrodechlorination of mono- and dichlorobenzenes.

2. Materials and Methods

2.1. Materials

In this study, the following reagents were used: copper (II) nitrate $Cu(NO_3)_2 \cdot 3H_2O$ (99.9%), palladium(II) chloride $PdCl_2$ (99.9%), sodium tetrahydroborate $NaBH_4$ (99.9%), sodium hydroxide NaOH, chlorobenzene C_6H_5Cl (99.5%), and 1,2-dichlorobenzene $C_6H_4Cl_2$ (99%). All reagents were purchased from Sigma Aldrich and used without additional purification. As a catalyst support, commercial wood-based activated carbon BAU-A (GOST 6217-74, Russia) was employed, which possessed the following characteristics: iodine adsorption activity of not less than 60%, ash content not exceeding 6%, and moisture content not exceeding 6%. For the modification of activated carbon, hydrochloric acid (GOST 11125-84, LLCMK MAGNA, Russia) was used according to the procedure described by Shaimardan et al [13].

2.2. Methods

2.2.1 Preparing the catalysts

In this study, the catalysts were synthesized using the wet impregnation method described by Hyeok et al. (Fig. 1) [32–34]. For the preparation of the Cu catalyst, 6.5 g of copper(II) nitrate was dissolved in 5 mL of deionized water, after which 10 g of AC_m was introduced into the solution and stirred vigorously for 10 minutes. The mixture was then placed in a desiccator for 4 hours to facilitate the sorption of Cu ions, followed by drying at 150 °C for 2 hours to remove excess water. To stabilize the Cu ions, the Cu^{2+}/ACm sample was calcined at 330°C for 4 hours. Subsequently, the reduction of Cu^{2+} in ACm was carried out by dissolving 1.6 g of sodium borohydride ($NaBH_4$) in 20 mL of distilled water. Subsequently, the $NaBH_4$ solution was added to a 50 mL aqueous-alcohol solution with a volume ratio of 30:70, and the mixture was stirred. To adjust the pH to ≤ 7, a 5 N NaOH solution was introduced. The $NaBH_4$ solution was slowly added to the Cu^{2+}/ACm suspension and stirred for 3 hours until the complete release of hydrogen. The resulting catalyst contained 10 wt.% of active Cu phase (10Cu/ACm).

The preparation of the Pd catalyst followed a similar procedure, where 20 mg of palladium (II) chloride was dissolved in 20 mL of an aqueous-alcoholic solution with a volume ratio of 30:70 (90% ethanol to water), and then mixed with 1 g of ACm under vigorous stirring. The obtained catalyst contained 5 wt.% of active Pd phase (5Pd/ACm). The bimetallic Pd–Cu catalyst was synthesized using the same procedure, with the difference that Pd^{2+}/ACm and Cu^{2+}/ACm suspensions were combined in a 3:7 ratio before the addition of the $NaBH_4$ solution. The final bimetallic catalyst contained 3 wt.% of active Pd phase and 7 wt.% of active Cu phase (3Pd–7Cu/ACm).

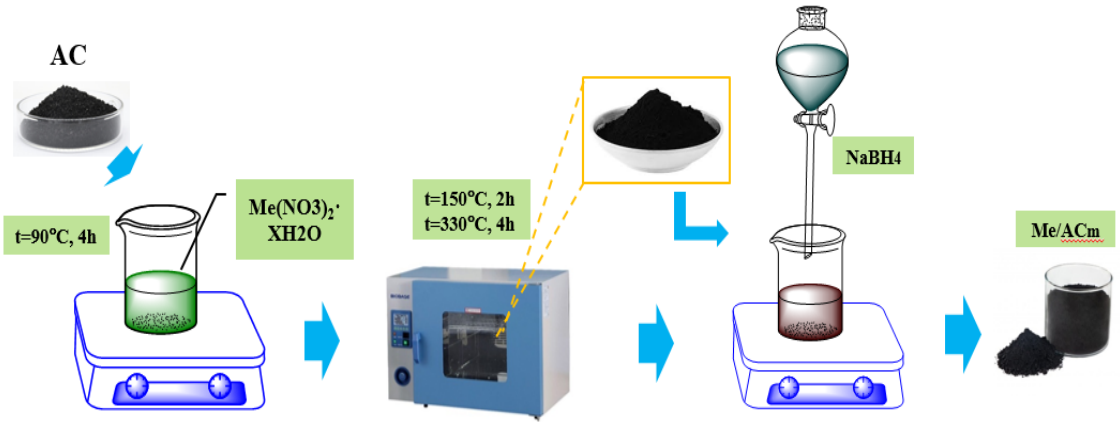

Figure 1 – Schematic for preparation of $10Cu/AC_m$, $5Pd/AC_m$ and3Pd-$7Cu/AC_m$ catalysts.---

2.2.2 FTIR analysis

Fourier-transform infrared (FTIR) spectroscopy was performed using an FTIR FT-801 spectrometer (Simex, Russia) with a resolution of 1 cm^{-1} in the range of 500–4000 cm^{-1}. Measurements were conducted at 25°C following the standard procedure, employing KBr pellets prepared at a 1:10 sample-to-KBr ratio. A total of 100 scans were collected for each spectrum. Prior to use, potassium bromide was finely ground and calcined at 200°C for 3 hours.

2.2.3 X-ray diffraction (XRD) analysis

The crystal structure of the samples was analyzed using an X'PertPRO diffractometer (Malvern Panalytical Empyrean, Netherlands) equipped with monochromatized CuKα radiation. Data were collected over the 2θ range of 10–45° with a step size of 0.02°. The operating conditions included an X-ray tube voltage of 45 kV, a current of 30 mA, and a counting time of 0.5 s per step.

2.2.4 Thermogravimetric analysis (TGA)

Thermal stability and decomposition behavior of the catalysts were investigated using an STA449C simultaneous thermal analyzer (NETZSCH, Germany) under an argon atmosphere. Measurements were conducted in the temperature range of 30–700°C with a heating rate of 10 ± 1°C/min. The initial sample mass was approximately 20 ± 2 mg.

2.2.5 Scanning and transmission electron microscopy (SEM and TEM)

The morphology and structure of the catalysts were characterized using a Crossbeam 540 high-vacuum scanning electron microscope (Zeiss, Germany). Elemental composition was determined by energy-dispersive X-ray spectroscopy (EDS, Thermo Fisher Scientific, USA). Transmission electron microscopy (TEM) images were obtained with a JEM-1400 microscope (JEOL, Japan), operating at an accelerating voltage of 120 kV, with a resolution of 0.38 nm, equipped with a Morada high-resolution CCD digital camera (Olympus, Japan). Prior to TEM, samples were ground in an agate mortar, dispersed in ethanol, and sonicated at 44 kHz using an UZDN-2T ultrasonic generator (Electron, Russia). A drop of the suspension was deposited on a perforated carbon-coated copper grid and dried before imaging. Particle size distributions and average particle diameters were determined statistically from TEM micrographs.

2.2.6 Adsorption porosimetry

Textural properties of the catalysts were determined by low-temperature nitrogen adsorption–desorption measurements using an Autosorb-1 analyzer (Quantachrome Instruments, USA). Before analysis, the samples were degassed under vacuum at 200–250°C for 3 hours. The Brunauer–Emmett–Teller (BET) method was applied to calculate specific surface area, with a measurement error of ±2.8%. Pore size distribution and total pore volume were derived from desorption isotherms using the Barrett–Joyner–Halenda (BJH) method.

2.2.7 Catalytic activity

Catalytic hydrodechlorination of chlorobenzene and 1,2-dichlorobenzene was carried out in an RVD-2-150 high-pressure reactor (Uoslab, Ukraine). The reaction mixture consisted of 1 mL of organochlorine compound, 0.1 g of catalyst, 3 mL of NaOH solution, and 1 mL of ethanol in a two-neck round-bottom flask [30]. Hydrogen gas was introduced at 50°C under 10 atm pressure, with magnetic stirring for 5 hours. After completion, the reaction mixture was washed with 10 mL of magnesium sulfate solution to precipitate sodium salts. A 1 mL aliquot of the treated solution was diluted with 19 mL of hexane for subsequent analysis.

2.2.8 Gas chromatography–mass spectrometry (GC–MS)

The hydrodechlorination products were analyzed using a 5975C GC/MS system (Agilent, USA) equipped with a GC–MSD quadrupole mass spectrometric detector (Agilent, USA). Operating conditions were as follows: electron ionization energy of 70 eV; HP-5MS quartz capillary column (30 m × 0.25 mm × 0.25 μm); helium as carrier gas; split ratio of 1:50; flow rate of 1.0 mL/min. The oven temperature program consisted of an initial temperature of 40°C (held for 3 min), followed by heating at 10°C/min to a maximum of 290°C, with a final holding time of 30 min.

3. Results and discussion

Physical and chemical characteristics of the 5Pd/ACm, 10Cu/ACm, and 3Pd–7Cu/ACm catalysts are presented below.

3.1. FTIR spectroscopy

In the FTIR spectra of 5Pd/AC_m, 10Cu/AC_m and 3Pd-7Cu/AC_m, in comparison to unmodified AC, the appearance of intense peaks in the region of 600-750 cm^{-1} and the absence of an absorption band in the region of 1713 cm^{-1}, related to C=O, are observed, which indicates a new bond in the catalysts, as seen in Figure 2.The data is in good agreement with previous studies. The most important difference in the FTIR spectra of the catalytic systems is the absence of the C=O vibration at 1713 cm^{-1}, which indicates the interaction of NPs and AC_m through the C–OH functional group.

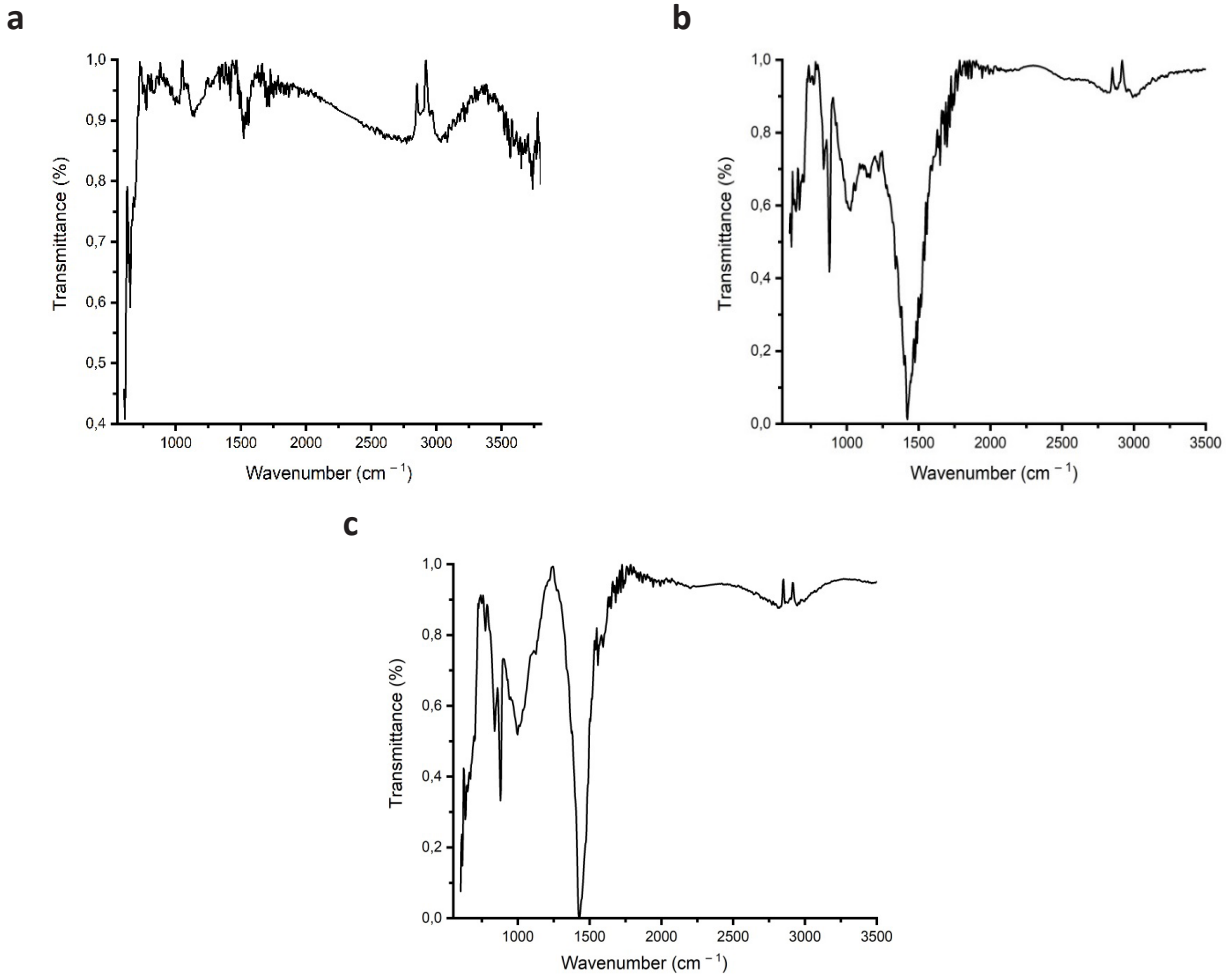

Figure 2 – The FTIR spectra of catalytic systems: a) 5Pd/AC_m; b) 10Cu/AC_m; and, c) 3Pd-7Cu/AC_m.

FTIR spectra demonstrate the disappearance of the C=O vibration at 1713 cm^{-1} together with the appearance of new bands in the 600–750 cm^{-1} region, which evidences chemical coordination of Pd and Cu nanoparticles specifically with carbonyl / carboxyl surface functionalities on ACm. XRD further confirms that the metals do not exist as independent separate phases: the presence of mixed reflections characteristic for Pd–Cu alloy formation shows that the two metals interact electronically at the atomic level, forming common crystallographic domains rather than isolated particles. Taken together, FTIR and XRD results indicate that the active phase is a true nanoalloy, strongly bonded to oxygen-containing anchoring sites of the HCl-modified carbon support, and this metal–metal–support coupling is the basis for the enhanced catalytic behavior observed.

3.2. XRD analysis

The X-ray diffraction (XRD) analysis of the 5Pd/AC_m catalyst reveals three distinct diffraction peaks at 2θ values of 23.6°, 43.5°, and 72.5°, which correspond to the Miller indices (003), (101), and (220), respectively. These peaks indicate that the catalyst exhibits a face-centered cubic lattice structure. This structural information is significant as it confirms the successful reduction of the $PdCl_2$ precursor to Pd NPs (Fig. 3, Table 1).

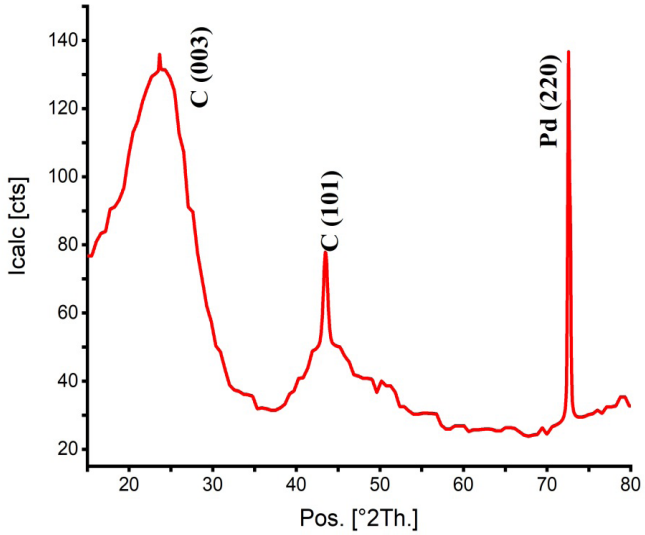

Figure 3 – X-ray diffraction pattern of 5Pd/AC_m catalyst.

Table 1 – Interplanar distance (d) of atoms in the 5Pd/AC_m catalyst.

Pos. [°2Th.]	Height [cts]	FWHM Left [°2Th.]	d-spacing [Å]	Rel. Int. [%]
23.6308	4.90	0.0900	3.76197	4.52
43.4566	19.83	0.5904	2.08245	18.31
72.5528	108.30	0.1968	1.30296	100.00

XRD analysis of 10Cu/AC_m revealed five diffraction peaks, with Miller indices at 2θ = 26.47 (020), 36.31 (111), 42.34 (121), 49.96 (020) and 72.58 (022) (Fig. 4, Table 2). The X-ray diffraction (XRD) pattern of the 10Cu/AC_m catalyst provides critical structural information. In the 2θ angle range of 50-80°, the pattern exhibits a series of reflections characteristic of a face-centered cubic (FCC) lattice, thereby confirming the presence of metallic copper (Cu). Additionally, in the 2θ angle range of 20-45°, the pattern reveals reflections indicative of cubic lattices, which demonstrate the presence of copper oxide (CuO).

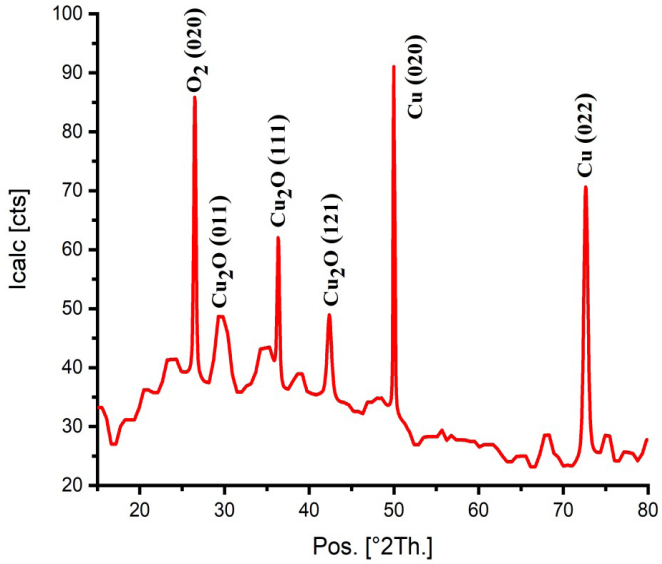

Figure 4 – X-ray diffraction pattern of 10Cu/AC_m catalyst.

Table 2 – Interplanar distance (d) of atoms in the 10Cu/AC_m catalyst.

Pos. [°2Th.]	Height [cts]	FWHM Left [°2Th.]	d-spacing [Å]	Rel. Int. [%]
26.4737	34.14	0.2952	3.36688	61.29
36.3197	17.76	0.2952	2.47358	31.89
42.3402	9.88	0.5904	2.13474	17.74
49.9641	55.70	0.1476	1.82542	100.00
72.5885	35.69	0.4920	1.30241	64.08

The crystal structure and phase characteristics of the 3Pd-7Cu/AC_m bimetallic catalyst are elucidated by five diffraction peaks, corresponding to the following Miller indices: 2θ = 26.49° (002), 36.88° (100), 43.14° (111), 62.51° (213), and 72.63° (022) (Fig.5, Table 3). The lattice parameter for palladium (Pd) is determined to be 3.36421 Å, which is closely aligned with the literature value of 3.890 Å. The copper (Cu) component exhibits a face-centered cubic (FCC) lattice, while the palladium (Pd) displays a hexagonal lattice structure. Moreover, the Pd-Cu alloy demonstrates a tetragonal lattice structure (Table 3).

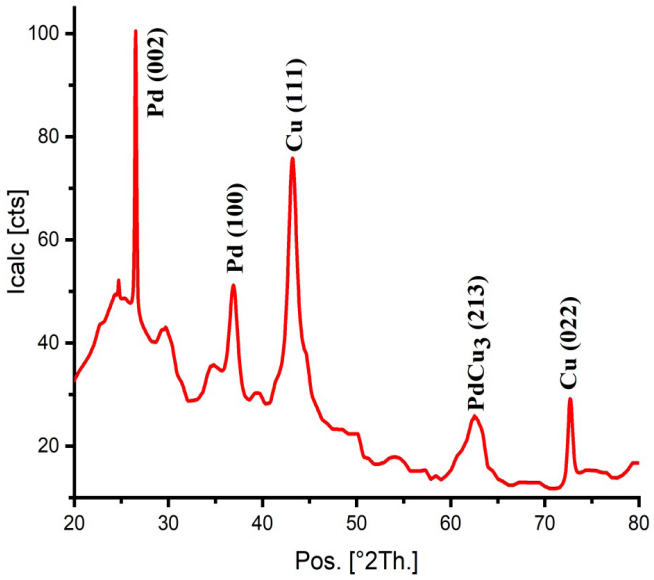

Figure 5 – X-ray diffractionof3Pd-7Cu/AC_m.

Table 3 – Interplanar distance (d) of atoms in the 3Pd-7Cu/AC_m catalyst.

Pos. [°2Th.]	Height [cts]	FWHM Left [°2Th.]	d-spacing [Å]	Rel. Int. [%]
26.4950	40.78	0.1968	3.36421	100.00
36.8896	14.00	0.9840	2.43666	34.32
43.1491	28.14	0.9840	2.09658	69.01
62.5193	0.79	0.0900	1.48444	1.94
72.6397	12.30	0.4920	1.30161	30.16

3.3. Thermogravimetric analysis

Thermogravimetric analysis established a sharp decrease in the mass of all samples of catalysts, which occurred in the temperature range of 30-130°C, due to the evaporation of surface adsorbed water (Fig. 6). Furthermore, gradual decrease in the mass of 5Pd/AC_m, 10Cu/AC_m and 3Pd-7Cu/AC_m was observed in the temperature range of 450-700°C, which was caused by the combustion of carbonaceous compounds (Figures 5a-d). The state of general equilibrium in the temperature range of 150-450^{0}C indicates the stability of the carboxyl, carbonyl and lactone groups, which is likely due to the interaction of metal ions with these specified functional groups.

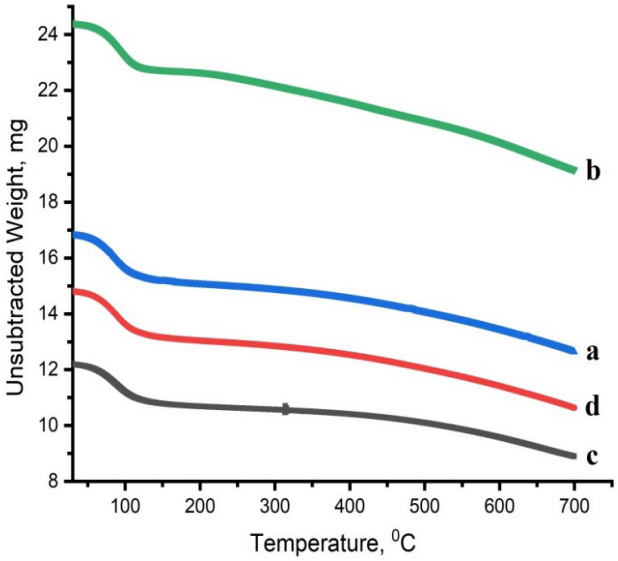

Figure 6 –TGA curves of AC_m alone and of the catalytic systems: a) AC_m; b) $5Pd/AC_m$; c) $10Cu/AC_m$; and, d) $3Pd\text{-}7Cu/AC_m$.

3.4. SEM and EDX analysis

Figures 6-8 present scanning electron micrographs of the $5Pd/AC_m$, $10Cu/AC_m$, and $3Pd\text{-}7Cu/AC_m$ catalysts. The $5Pd/AC_m$ catalyst exhibits a relatively smooth surface texture, spherical palladium nanoparticles (Pd NPs) with a uniform size distribution ranging from 18.04 to 19.50 nm (Fig. 7). Energy dispersive spectroscopy (EDX) analysis, integrated with SEM data, confirms that the palladium content in this catalyst is 3.9%.

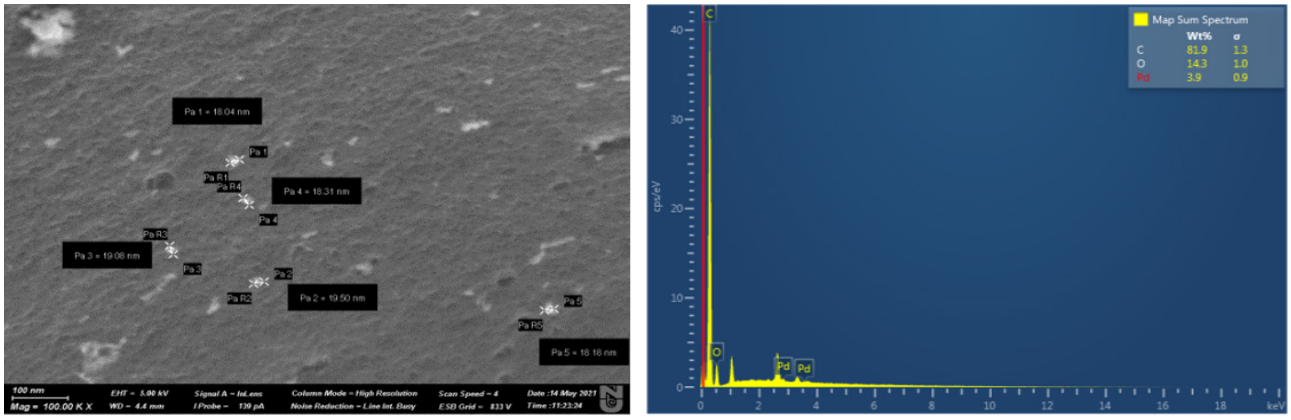

Figure 7 – SEM image and energy-dispersive X-ray (EDX) spectrum of the of $5Pd/AC_m$ catalyst.

In the 10Cu/AC$_m$ catalyst, SEM imaging reveals a rougher surface texture with copper nanoparticles (Cu NPs) ranging in size from 18.58 to 29.56 nm (Fig. 8). EDX data indicate a high carbon content of 79.9 wt.% and an oxygen content of 19.2 wt.%, while the copper content is measured at 10%

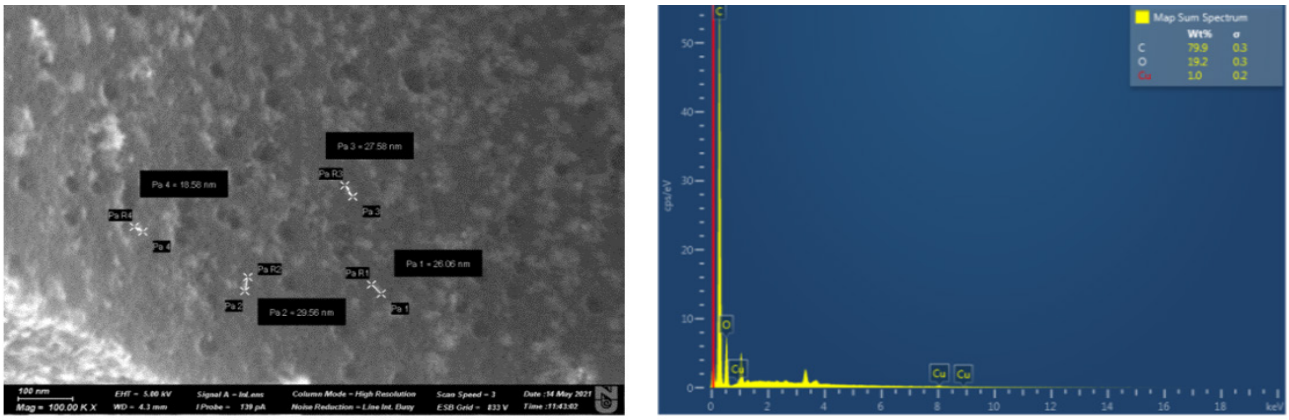

Figure 8 – SEM image and energy-dispersive X-ray (EDX) spectrum of the 10Cu/AC$_m$catalyst

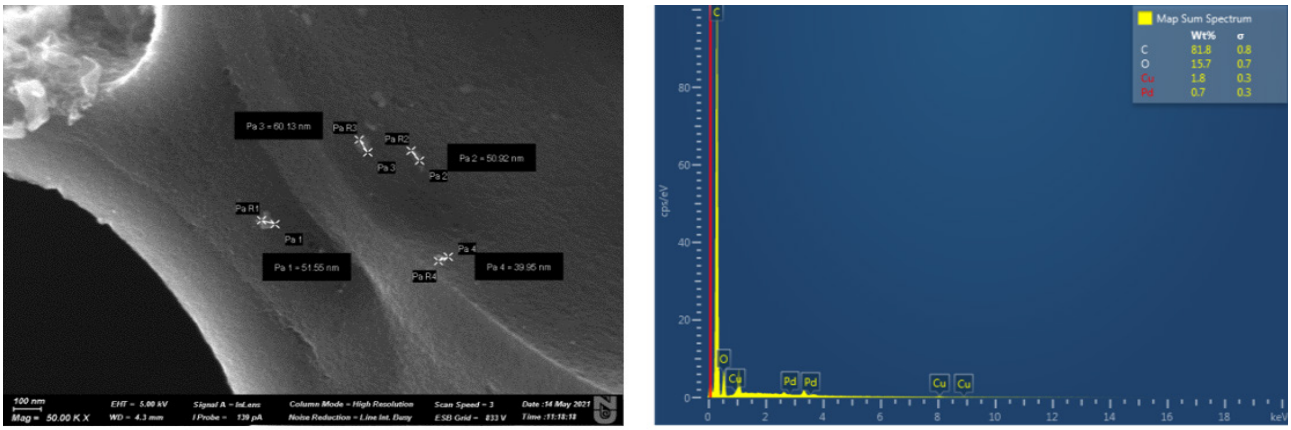

Figure 9 – SEM image and energy-dispersive X-ray (EDX) spectrum of the of 3Pd-7Cu/AC$_m$catalyst.

The 3Pd-7Cu/AC$_m$ bimetallic catalyst exhibits a more uniform texture compared to the monometallic catalysts, with particle sizes approximately twice as large, ranging from 39.95 to 60.13 nm (Fig. 9). EDX analysis confirms the presence of copper (Cu) and palladium (Pd) at concentrations of 1.8 wt.% and 0.7%, respectively. Figures 10-12 depict the TEM images of 5Pd/AC$_m$, 10Cu/AC$_m$, and 3Pd-7Cu/AC$_m$.

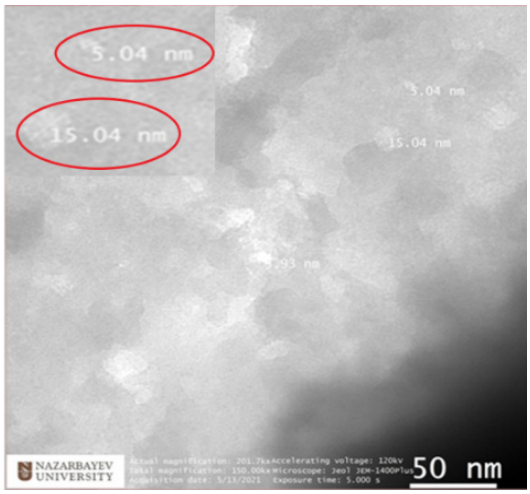

Figure 10 – TEM image of 5Pd/AC_m catalyst.

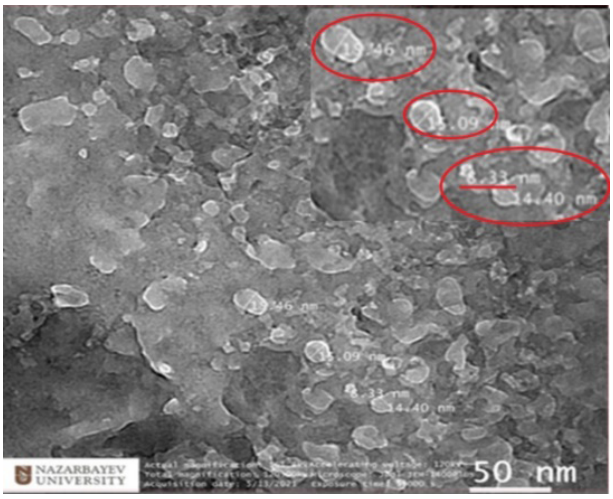

Figure 11 – TEM image of 10Cu/AC_mcatalyst.

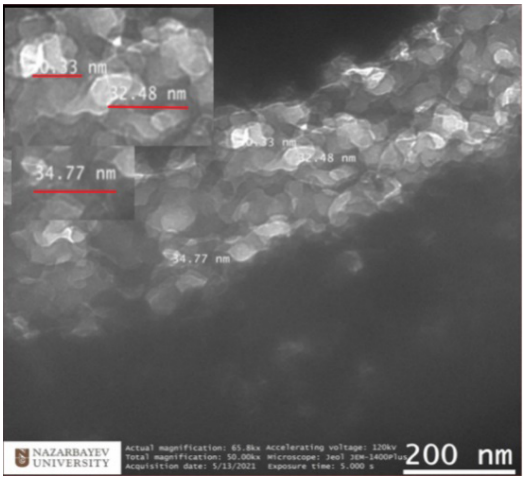

Figure 12 – TEM image of 3Pd-7Cu/AC_m catalyst.

3.5. TEM analysis

Transmission electron microscopy reveals that Pd nanoparticles form on the surface layer (Fig. 10) and exhibit diverse geometries and dimensions, ranging from 5 to 15 nm. The 10Cu/AC_m sample contains both small and large Cu nanoparticles, with sizes ranging from 8 to 19 nm, displaying various shapes and distributed uniformly across the entire surface of the catalyst (Fig. 11). The 3Pd-7Cu/AC_m bimetallic catalyst features larger nanoparticles in the range of 30 to 34 nm, which aggregate to form agglomerates (Fig. 12).

3.6. BET analysis

Table 4 shows the indicators of the specific surface area of AC_m alone and the three catalytic systems, calculated using the multipoint BET method, including the total pore volume and characteristics of the micropores. Further, the pore size distribution, surface area, and nitrogen adsorption-desorption isotherms of the catalytic systems are shown in Figures 13-14.

The catalysts synthesized exhibit a specific surface area ranging from 371.4 to 672.1 m²/g, which is 1.6 to 2.9 times higher than that of the AC_m support (Table 4). Additionally, there is a notable reduction in pore size accompanied by a substantial increase in total pore volume. Upon incorporation of Pd nanoparticles into the modified carrier, the specific surface area reaches 371.4 m²/g. In contrast, catalysts containing Cu nanoparticles show a specific surface area twice as large as that of Pd, at approximately 672.1 m²/g. The 3Pd-7Cu/AC_m catalytic system demonstrates a significant nearly two-fold increase in

specific pore surface area compared to the modified carrier (Table 4), consistent with findings from prior research [12]. All catalysts exhibit an increase in total pore volume, measured at 36.6, 73.9, and 65.6 ml/g for 5Pd/AC_m, 10Cu/AC_m, and 3Pd-7Cu/AC_m, respectively, indicating a well-developed porous structure. This expansion suggests an enhanced capability for adsorbing pollutants due to an increase in available adsorption sites. The pore sizes (Dv(r)) of the catalysts is seen to have decreased by 6.37-6.4 times, as compared to those of the AC_m carrier [12]. The order of reduction is: 10Cu/AC_m>3Pd-7Cu/AC_m>5Pd/AC_m (Table 4). The increase in the specific surface area and pore volume of all the catalysts is accompanied by a corresponding decrease in pore size, which is in the range of 19.084 nm, 19.168 nm and 19.070 nm for 5Pd/AC_m, 10Cu/AC_m and 3Pd-7Cu/AC_m, respectively, as compared to the carrier [12] (Table 4). This result may be due to the localization of Pd, Cu and Pd-Cu inside the pores of AC_m.

Table 4 – Specific surface area, size, total pore volume of AC_m; 5Pd/AC_m,; 10Cu/AC_m; 3Pd-7Cu/AC_m.

Sample	Surface area, m^2/g	Poresize, nm	Porevolume, ml/g
AC_m[12]	233.8	122.1	0.19
5Pd/AC_m	371.4	19.0	36.6
10Cu/AC_m	672.1	19.1	73.9
3Pd-7Cu/AC_m	600.4	19.07	65.6

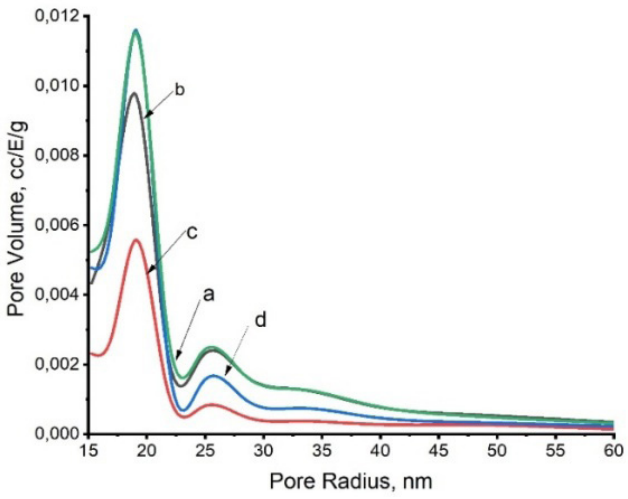

Figure 13 – Pore size distribution of different catalysts:
a) AC_m; b) 5Pd/AC_m; c) 10Cu/AC_m; and, d) 3Pd-7Cu/AC_m.

Further examination of the textural properties of the synthesized catalysts reveals distinct pore structures compared to the AC_m carrier (Fig. 13). The N_2 adsorption isotherm for all catalysts exhibits a type IV behavior, characterized by rapid and uniform nitrogen adsorption. The initial curves of these isotherms indicate the presence of micropores in all samples. At higher P/Po values, a slight capillary condensation appears on the isotherm, accompanied by a characteristic H4-type hysteresis loop. The pronounced wide hysteresis loop, classified as type IV according to IUPAC guidelines, reaffirms the uniform pore size and mesoporous nature of the materials.

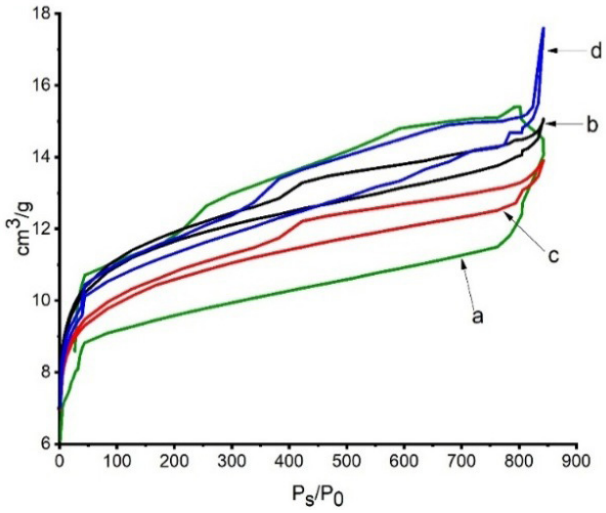

Figure 14 – N_2 adsorption-desorption isotherms of catalysts: a) AC_m; b) $5Pd/AC_m$; c) $10Cu/AC_m$; and d) $3Pd\text{-}7Cu/AC_m$.

3.7. Catalytic hydrodechlorination of chlorobenzene and 1,2-dichlorobenzene

The $5Pd/AC_m$, $10Cu/AC_m$ and $3Pd\text{-}7Cu/AC_m$ catalysts were tested using the model hydrodechlorination reactions of chlorobenzene and 1,2-dichlorobenzene, separately, in 10 ml ethanol, at a temperature of 50^0C and P_{H2} of 10 atm, over a period of 5 hrs. The data on the catalytic activity for the neutralization of the organohalogen substances are given in Table 5 and Figures 15-17.

Table 5 – Hydrodechlorination of chlorobenzene and 1,2-dichlorobenzene, using the $5Pd/AC_m$, $10Cu/AC_m$ and $3Pd\text{-}7Cu/AC_m$ catalysts.

Sample	Chlorobenzene		1,2-dichlorobenzene	
	Conversionproduct	Conversion, %	Conversionproduct	Conversion, %
$5Pd/AC_m$	Benzene	82,90	Benzene	86,74
$10Cu/AC_m$	Benzene	70,20	Benzene	80,30
$3Pd\text{-}7Cu/AC_m$	Benzene	93,94	Benzene	89,79

To further contextualize these results, Table 6 compares the catalytic performance of the 3Pd–7Cu/ACm catalyst with representative Pd-Cu based systems previously reported in the literature. This comparative overview clearly demonstrates that the Cu-rich 3Pd–7Cu/ACm composition provides competitive or even superior hydrodechlorination activity, while maintaining significantly lower Pd loading.

Table 6 – Comparison of hydrodechlorination performance of Pd–Cu catalysts with previously reported systems.

Catalyst System	Metal Loading (wt%)	Support Type	Chlorobenzene Conversion (%)	1,2-Dichlorobenzene Conversion (%)	Main Products	Findings
3Pd–7Cu/ ACm	3 Pd, 7 Cu	HCl-modified activated carbon	93.94	89.79	Benzene	Highest conversions with reduced Pd loading due to Cu-rich nanoalloy and modified support

Continuation of the table

Catalyst System	Metal Loading (wt%)	Support Type	Chlorobenzene Conversion (%)	1,2-Dichlorobenzene Conversion (%)	Main Products	Findings
5Pd/ACm	5 Pd	HCl-modified activated carbon	82.90	86.74	Benzene	Monometallic Pd catalyst, moderate conversions
10Cu/ACm	10 Cu	HCl-modified activated carbon	70.20	80.30	Benzene	Cu catalyst shows lower conversion compared to Pd or bimetallic
Pd–Cu/ Coal-Based AC	~10 Pd	Coal-based activated carbon	80–100	-	-	Previously reported high activity with higher Pd content
Pd–Fe/ GAC	Pd ~2-3 nm layer on Fe NPs	Granular activated carbon	~90 for PCB	-	Biphenyl	Bimetallic Pd-Fe catalysis, complex synthesis
Pd/C-Et3N	10 Pd	Modified carbon (triethylamine)	100 for PCB	-	Biphenyl	Complete decomposition of PCBs; high Pd loading
Cu/PVP–AC	~5 Cu	AC stabilized with PVP	94.46	-	Benzene	Copper-only catalyst with stabilizer shows high conversion
Pd/C (various)	10 Pd	Various activated carbons	80–100	-	Various	Widely studied Pd catalysts for hydrodechlorination with high activity

3.8. Gas chromatography-mass spectrometry analysis

The conversion of chlorobenzene through hydrodechlorination using 5Pd/AC_m, 10Cu/AC_m and 3Pd-7Cu/AC_m is 82.9%, 70.20 and 93.94%, respectively (Table 5, Figures 14a-16a). Hydrodechlorination of 1,2-dichlorobenzene using 5Pd/AC_m, 10Cu/AC_m and 3Pd-7Cu/AC_m is 86.74%, 80.30% and 89.79%, respectively (Table 5, Figures 14b-16b). In both cases, the conversion product was benzene. The bimetallic catalyst, 3Pd-7Cu/AC_m, showed the greatest activity in the hydrodechlorination of both organohalogens, with a conversion rate of 93.94% and 89.79%, respectively. The order of increasing catalytic activity in the hydrodechlorination of organohalogen substances is 10Cu/AC_m<3Pd/AC_m<3Pd-7Cu/AC_m.

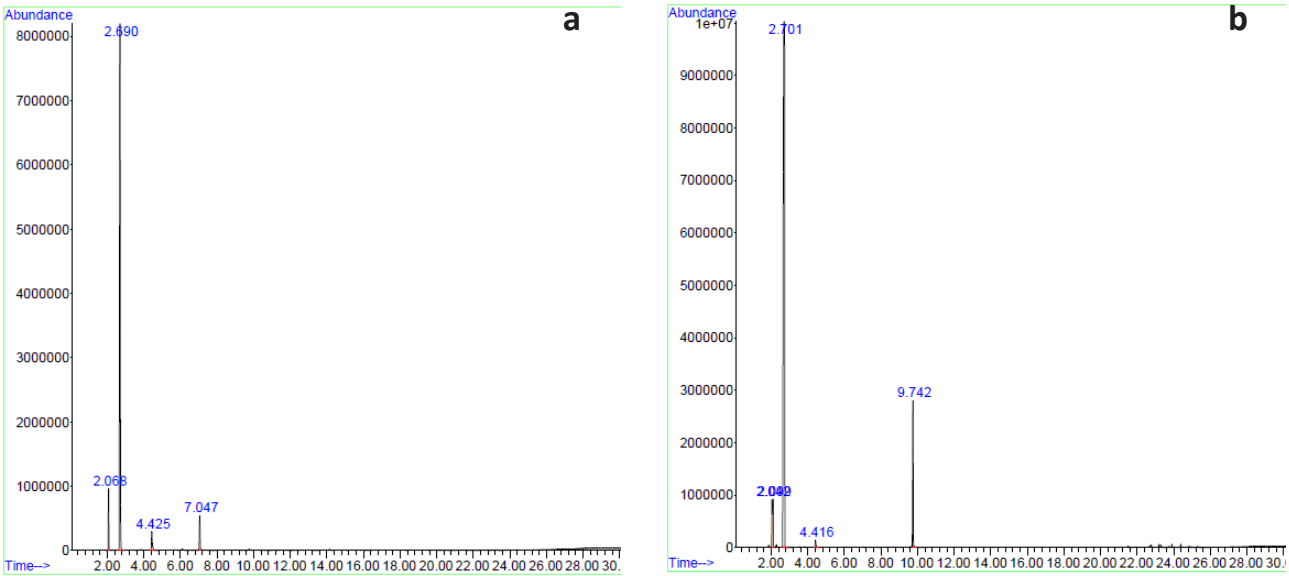

Figure 15 – Chromatogram of the hydrodechlorination products of:
a) chlorobenzene; b) 1,2-dichlorobenzene, using 5Pd/AC_m (10 mg) at a temperature of 50^{0}C.

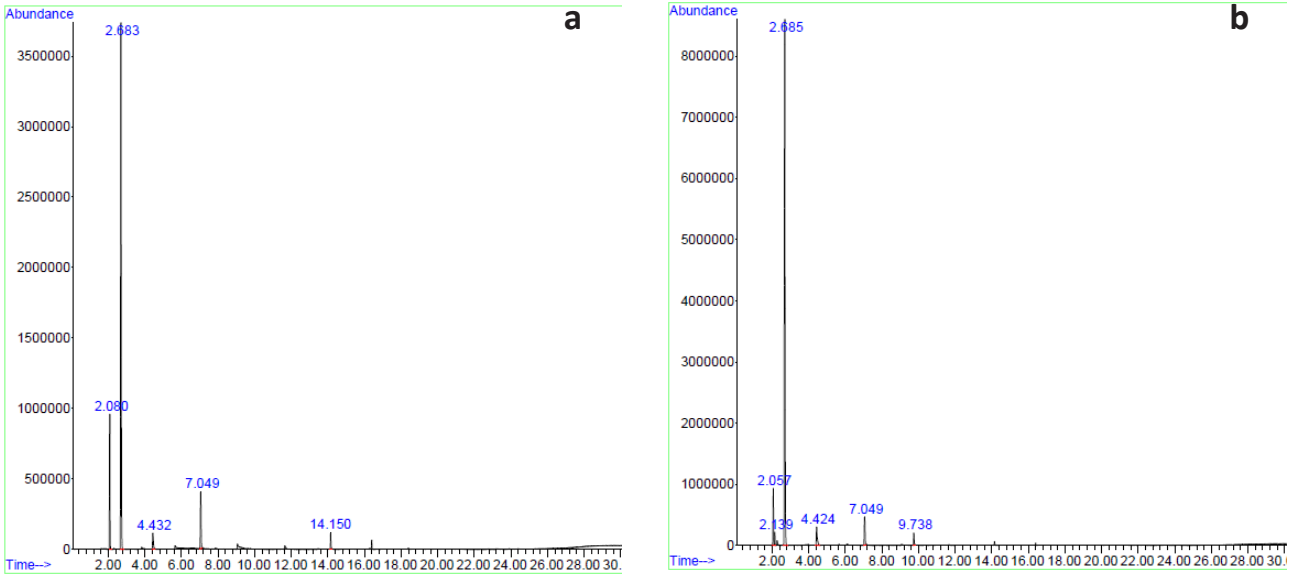

Figure 16 – Chromatogram of the hydrodechlorination products of:
a) chlorobenzene; b) 1,2-dichlorobenzene, using 10Cu/AC_m catalyst (10.0 mg) at a temperature of 50^0C.

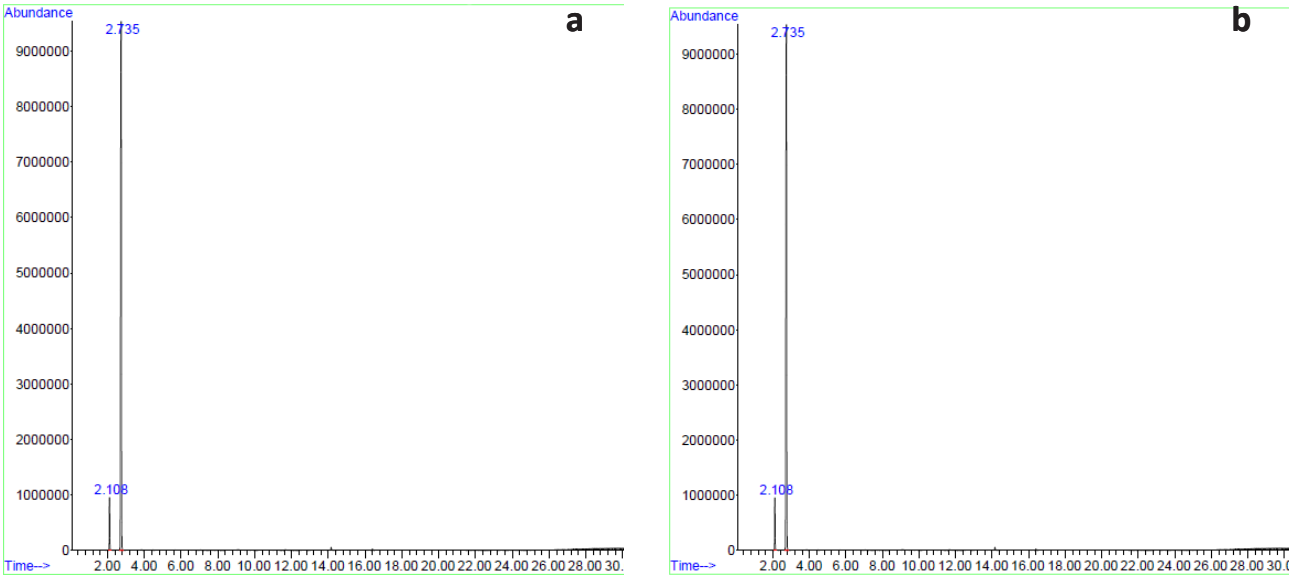

Figure 17 – Chromatogram of the hydrodechlorination products of:
a) chlorobenzene; b) 1,2-dichlorobenzene, using 3Pd-7Cu/AC_m catalyst (10 mg) at a temperature of 50^0C.

4. Conclusions

Three dehydrochlorination catalysts were synthesized on modified activated carbon (AC_m), using Pd and Cu nanoparticles (NPs), both alone and as a bimetal. Based on prior research, the following combinations were selected, using estimations of both cost and effectiveness: 5% Pd (5Pd/AC_m), 10% Cu (10Cu/AC_m), and 3% Pd with 7% Cu (3Pd-7Cu/AC_m). As per FTIR, TGA and EDX analyses, the NPs are able to connect with the AC_m carrier at the carboxyl and carbonyl functional groups. The pore sizes of the resulting catalysts have a range of 19.070 to 19,168 nm, which is 100 times smaller than that of the AC_m carrier alone. Further, the surface areas of the catalysts were found to be in the range of 371.748 to 672,132 m^2/g, which is 1.6-2.9 times higher than that of AC_m. These results on the pore structures of the catalysts demonstrate good development, allowing for an increased number of sites to adsorb persistent organic

pollutants (POPs). Whereas all the catalysts showed effectiveness in dehydrochlorinating chlorobenzene and 1,2-dichlorobenzene, separately, into benzene, the bimetallic catalyst, 3Pd-7Cu/AC_m, demonstrates the best results, with conversion rates of 93.94% and 89.79%, respectively.

The usage of inexpensive metallic NPs, like Cu, as catalysts on an AC_m carrier allows for a reduction in the amount of more expensive materials, such as Pd. The need for efficient and cost-effective catalysts to decrease the number of POPs is of great importance to all nations, especially in Kazakhstan, which faces serious problems created by both the industrial and agricultural sectors regarding POPs. This is in accordance with the WHO Convention on Persistent Organic Pollutants, which targets the reduction of both existing and future halogenated organic compounds. Furthermore, as Kazakhstan is already known for its petroleum production, the use of new types of nanocatalysts that regenerate the hydrocarbon component of halogenated molecules can create a synergistic relationship among the petroleum, agricultural, chemical and research sectors of the country. Finally, the current research team hopes to particularly find opportunities for this technology in the cleanup of hazardous areas that have been negatively affected by both past and recent application of halogenated organic compounds.

A deeper mechanistic explanation of the catalytic pathway can be formulated by considering the specific roles of Pd, Cu, and the HCl-modified carbon surface. According to our FTIR results, both Pd and Cu nanoparticles are bound to carboxyl and carbonyl functionalities of the modified activated carbon. This anchoring not only stabilizes the nanoparticles, but also electronically couples them to the support, creating an interface that facilitates H2 activation and stabilizes surface hydride species. XRD analysis confirms the formation of Pd–Cu alloy phases, which is a direct structural indicator of electronic interaction between the two metals at the atomic level. In Pd–Cu nanoalloys, the presence of Cu modifies the electronic density of Pd: electron donation from Cu to Pd shifts the d-band center of Pd to lower energy, which is known to weaken the Pd–Cl interaction. As a result, the C–Cl bond cleavage pathway becomes energetically more favorable, and surface poisoning by strongly adsorbed chlorides is reduced. Pd remains the primary site for H2 dissociation, while Cu facilitates electron transfer steps and stabilizes reactive intermediates, which together increases the overall turnover for hydrodechlorination. The modified carbon support additionally contributes by providing high surface area mesoporosity and a high density of oxygen-containing groups, which improves nanoparticle dispersion and suppresses sintering or growth during reaction.

Thus, the high activity of the 3Pd–7Cu/ACm catalyst can be explained mechanistically by the combination of (I) alloy-driven electronic tuning of Pd by Cu, (II) more efficient H_2 activation–transfer sequence at the bimetallic interface, and (III) stronger metal–support interactions induced by HCl modification of the carbon. These three effects act synergistically, and this explains why a Cu-rich formulation with reduced Pd loading can achieve higher conversion than monometallic Pd or Cu catalysts.

Acknowledgments. The authors would like to thank the management and staff of the Institute of Atomic Energy, Branch RSE NNC RK, Kurchatov, Kazakhstan, for providing the necessary infrastructure and resources for carrying out this research. The authors are also grateful to the Scientific Center of Composite Materials, Almaty, Kazakhstan, and Satbayev University, Almaty, Kazakhstan, for their technical support and contributions. Special thanks are extended to Mahatma Gandhi University, Kottayam, India, and Government Postgraduate College Rajouri, Jammu and Kashmir, India, for providing the facilities for material synthesis and analysis. The authors also appreciate the contribution of Mprex Healthcare Pvt., Ltd. Pune, India, for supplying the extract samples used in this study.

Funding. This research has been funded by the Science Committee of the Ministry of Science and Higher Education of the Republic of Kazakhstan (Grant No. BR21882200).

References

1. Stockholm Convention on Persistent Organic Pollutants (POPs) as amended in 2009. Text and An-nexes. – 2009. – P. 1–64. – Available at: https://www.pops.int/Portals/0/Convention%20text/UNEP-POPS-COP-CONVTEXT-2009.En.pdf (Available online on December 16, 2025).

2. Shaimardan E., Kabdrakhmanova S. K., Beisebekov M. M., Selenova B. S., Imangazinova Zh., Sydykbayeva S. Nickel nanocatalyst for hydrodechlorination of polychlorinated biphenyls // Bulletin of the National Nuclear Center of the Republic of Kazakhstan. – 2023. – Vol. 2. – Pp. 74–81. https://doi.org/10.52676/1729-7885-2023-2-74-81

3. Detlev F., Karsten K., Katrin M., Dieter K. F. Hydrodechlorination of chloroorganic compounds in ground water by palladium catalysts // Catalysis Today. – 2003. – Vol. 82. – Pp. 105–118. https://doi.org/10.1016/S0920-5861(03)00208-6

4. Castillo C., García-Muñoz P., Pérez-Ramírez J., Martín-Martínez F. Advances in hydrodechlorina-tion technologies for diclofenac removal: A comprehensive review // Molecules. – 2025. – Vol. 30, No. 16. – Art. 3332. https://doi.org/10.3390/molecules30163332

5. Urbano F. J., Marinas J. M. Hydrogenolysis of organohalogen compounds over palladium supported catalysts // Journal of Molecular Catalysis A: Chemical. – 2001. – Vol. 173, No. 1–2. – Pp. 329–345. https://doi.org/10.1016/S1381-1169(01)00157-1

6. de Pedro Z. M., Diaz E., Mohedano A. F., Casas J. A., Rodriguez J. J. Compared activity and stabil-ity of Pd/Al_2O_3 and Pd/AC catalysts in 4-chlorophenol hydrodechlorination in different pH media // Applied Catalysis B: Environmental. – 2011. – Vol. 103. – Pp. 128–135. https://doi.org/10.1016/j.apcatb.2011.01.018

7. Lan L., Liu Y., Liu S., Ma X., Li X., Dong Z., Xia C. Effect of the supports on catalytic activity of Pd catalysts for liquid-phase hydrodechlorination/hydrogenation reaction // Environmental Technology. – 2019. – Vol. 40, No. 12. – Pp. 1615–1623. https://doi.org/10.1080/09593330.2018.1426645

8. Keane A. M. Supported transition metal catalysts for hydrodechlorination reactions // ChemInform Abstract. – 2011. – Vol. 3. – Pp. 800–821. https://doi.org/10.1002/chin.201137243

9. Benítez L. J., Del A. G. Total hydrodechlorination of industrial transformer oil on metal-supported catalysts // Chemical Engineering Communications. – 2009. – Vol. 196, No. 10. – Pp. 1217–1226. https://doi.org/10.1080/00986440902831888

10. Janiak T., Janina O. Effectiveness and stability of commercial Pd/C catalysts in the hydrodechlo-rination of meta-substituted chlorobenzenes // Applied Catalysis B: Environmental. – 2009. – Vol. 92. – Pp. 384–392. https://doi.org/10.1016/j.apcatb.2009.08.018

11. Mitoma Y., Katayama Y., Simion C. Mechanistic considerations on the hydrodechlorination process of polychloroarenes // IntechOpen. – 2018. https://doi.org/10.5772/intechopen.79083

12. Baktygerey S. B., Mussabek G., Zhylkybayeva N., et al. Palladium catalysts supported on car-bonized porous silicon for H_2/O_2 recombination // Physical Sciences and Technology. – 2023. – Vol. 10, No. 3–4. – Pp. 40–47. https://doi.org/10.26577/phst.2023.v10.i2.05

13. Shaimardan E., Kabdrakhmanova S. K., Beisebekov M. M., et al. Influence of liquid-phase oxida-tion of activated carbon "BAU-A" grade with hydrogenic acid on its surface structure // Bulletin of the National Nuclear Center of the Republic of Kazakhstan. – 2023. – Vol. 3(95). – Pp. 96–101. https://doi.org/10.52676/1729-7885-2023-3-96-102

14. Kabdrakhmanova S., Shaimardan E., Akatan K., et al. Preparation and characterization of the catalyst based on the copper nanoparticles // International Journal of Nanoscience and Nanotechnology. – 2022. – Vol. 18, No. 1. – P. 1–10. https://www.ijnnonline.net/article_249799_fd00a59e31d5e0e9690dfff364998c2b.pdf

15. Mussabek G., Diyuk V.E., Zaderko A.N., Afonin S., Baktygerey S., Taurbayev Ye., Yermukhamed D., Zhylkybayeva N., Yessengereyeva N., Lisnyak V.V. Thermal fluorination of nanoporous activated carbon mediated by freons // Diamond and Related Materials. -2025. -Vol. 155. -Art. 112197. https://doi.org/10.1016/j.diamond.2025.112197

16. Zhumadilov R., Zhumadilov B., Nemkayeva R., et al. In-situ Raman analysis of carbon nanowalls during electrochemical measurement // Physical Sciences and Technology. – 2025. – Vol. 12, No. 1–2. – Pp. 57–67. https://doi.org/10.26577/phst20251216

17. Jujjuri E., Ding E., Shore S. G., Keane M. A. Synthesis and characterization of novel silica-supported Pd/Yb bimetallic catalysts: Application in gas-phase hydrodechlorination and hydrogenation // Journal of Catalysis. – 2006. – Vol. 239. – Pp. 486–500. https://doi.org/10.1016/j.jcat.2006.02.022

18. Mussabek G., Baktygerey S., Taurbayev Ye., Yermukhamed D., Zhylkybayeva N., Zaderko A.N., Diyuk V. E. Afonin S., Yar-Mukhamedova G., Mariychuk R.T., Grishchenko L. M., Kanuchova M., Lisnyak V.V. Surface chemistry and catalytic activity in H_2O_2 decomposition of pyrolytically fluoralkynated activated carbons // RSC Advances. – 2024. – Vol.14. -Art. 29052. https://doi.org/10.1039/d4ra04883k

19. Rodriguez J. G., Lafuente A., Cristóbal de los Ríos. Thermal analysis of 1,4-di[n'-(quinolyl)]buta-1,3-diynes, structure, and topo-oligomerization // Journal of Polymer Science Part A: Polymer Chemistry. – 2004. – Vol. 42, No. 23. – P. 6031–6040. https://doi.org/10.1002/pola.20441

20. Lorenc-Grabowska E., Yperman J., Gryglewicz G., Hoste S., Carleer R. Study on hydrodechlorina-tion of polychlorinated biphenyls during reductive pyrolysis in the presence of a catalyst // Fuel. – 2006. – Vol. 85, No. 3. – P. 374–381. https://doi.org/10.1016/j.fuel.2005.07.002

21. Kume A., Monguchi Y., Hattori K., Nagase H., Sajiki H. Pd/C-catalyzed practical degradation of PCBs at room temperature // Applied Catalysis B: Environmental. – 2008. – Vol. 81, No. 3–4. – P. 274–282. https://doi.org/10.1016/j.apcatb.2007.12.019

22. Nurbolat S. T., Gabdullin M., Kalkozova Z., Mirzaeian M., Abdullin K. Capacitive electrodes based on a combination of activated carbon and graphene // Physical Sciences and Technology. – 2022. – Vol. 9, No. 3–4. – P. 18–24. https://doi.org/10.26577/phst.2022.v9.i2.03

23. Xu Y., Zhang W.-X. Subcolloidal Fe/Ag particles for reductive dehalogenation of chlorinated ben-zenes // Industrial & Engineering Chemistry Research. – 2000. – Vol. 39, No. 7. – P. 2238–2244. https://doi.org/10.1021/ie9903588

24. Mekhaev A. V., Pervova M. G., Taran O. P., Simakova I. L., Parmon V. N. Pd/Sibunit as efficient hydrogen transfer catalyst in hydrodechlorination of polychlorobiphenyls // Russian Journal of Organic Chemistry. – 2014. – Vol. 50, No. 6. – P. 900–901. https://doi.org/10.1134/S1070428014060244

25. Mekhaev A. V., Pervova M. G., Taran O. P., et al. Liquid-phase dechlorination of toxic man-made products using nanodispersed palladium catalysts Sibunit // Chemistry for Sustainable Development. – 2011. – Vol. 19. – Pp. 173–180.

26. Beall G. W., Kuanyshbekov T. K., Tulegenova M. A. Graphene produced by carbon diffusion through nickel foil // Physical Sciences and Technology. – 2018. – Vol. 5, No. 3–4. – P. 37–42. https://doi.org/10.26577/phst-2018-2-156

27. Korte N. E., West O. R., Liang B. G., Zutman J. L., Fernando Q. The effect of solvent concentra-tion on the use of palladized-iron for the step-wise dechlorination of polychlorinated biphenyls in soil ex-tracts // Waste Management. – 2002. – Vol. 22, No. 3. – P. 343–349. https://doi.org/10.1016/S0956-053X(01)00050-2

28. Murena F., Schioppa E., Gioia F. Catalytic hydrodechlorination of a PCB dielectric oil // Environ-mental Science & Technology. – 2000. – Vol. 34. – P. 4382–4385. https://doi.org/10.1021/es000015x

29. Guo-Bin L., Tsukinoki T., Kanda T., Mitoma Y., Tashiro M. Organic reaction in water. Part 2. A new method for dechlorination of chlorobiphenyls using a Raney Ni–Al alloy in dilute aqueous alkaline solution // Tetrahedron Letters. – 1998. – Vol. 39. – P. 5991–5994. https://doi.org/10.1016/S0040-4039(98)01230-1

30. Xia C. H., Liu Y., Xu J., et al. Catalytic hydrodechlorination reactivity of monochlorophenols in aqueous solutions over palladium/carbon catalyst // Catalysis Communications. – 2009. – Vol. 10. – P. 456–458. https://doi.org/10.1016/j.catcom.2008.10.021

31. Calvo L., Gilarranz M. A., Casas J. A., Mohedano A. F., Rodriguez J. J. Hydrodechlorination of alachlor in water using Pd, Ni and Cu catalysts supported on activated carbon // Applied Catalysis B: Envi-ronmental. – 2008. – Vol. 78. – P. 259–266. https://doi.org/10.1016/j.apcatb.2007.09.028

32. Messerle V., Ustimenko A. Plasmatron with renewable carbon nanostructured covering of elec-trodes // Physical Sciences and Technology. – 2014. – Vol. 1, No. 1. – P. 43–47. https://doi.org/10.26577/phst-2014-1-13

33. Das D., Samal D. P., Meikap B. Preparation of activated carbon from green coconut shell and its characterization // Journal of Chemical Engineering & Process Technology. – 2015. – Vol. 6. – P. 248. https://doi.org/10.4172/2157-7048.1000248

34. Shimodaira N., Masui A. Raman spectroscopic investigations of activated carbon materials // Journal of Applied Physics. – 2002. – Vol. 92. – P. 902–909. https://doi.org/10.1063/1.1487434

Information about authors:

Mazhyn K. Skakov – Dr. Sci. (Phys. & Math.), Professor, Academician of KazNAEN, Chief Researcher at the Branch of the National Nuclear Center of the Republic of Kazakhstan, Professor of Physics and Technology at NAO VKU named after S. Amanzholov (Kurchatov, Kazakhstan, e-mail: skakov@nnc.kz, skakovmk@mail.ru).

Alseit Amirov – MSc, Researcher at the Satbayev University (Almaty, Kazakhstan, e-mail: alseit.amirov@gmail.com).

Ainur K. Kabdrakhmanova – PhD, Senior Researcher at the Satbayev University (Almaty & Astana, Kazakhstan, e-mail: ainurkabdrahmanova@mail.ru).

Nodira Toshkuvatova – MSc, Researcher at the Samarkand State University named after Sh. Rashidov (Samarkand, Uzbekistan, e-mail: nodira.toshkuvatova@gmail.com).

Aktam T. Khalmanov – PhD, Researcher at the Samarkand State University of Architecture and Construction named after Mirzo Ulugbek (Samarkand, Uzbekistan, e-mail: a-xalmanov@umail.uz).

Arman Zh. Miniyazov – PhD, Director of the Center for Technological Competence in the Field of Hydrogen Energy, Institute of Atomic Energy, NNC RK (Kurchatov, Kazakhstan, e-mail: miniyazov@nnc.kz).

Viktor V. Baklanov – PhD, Associate Professor, First Deputy Director of the Branch Institute of Atomic Energy, NNC RK (Kurchatov, Kazakhstan, e-mail: baklanov@nnc.kz).

Yerbolat T. Koyanbayev – PhD, Researcher at the Branch Institute of Atomic Energy, NNC RK (Kurchatov, Kazakhstan, e-mail: erbol@nnc.kz).

Nuriya M. Mukhamedova – PhD, Head of Laboratory of Advanced Materials, Branch Institute of Atomic Energy, NNC RK (Kurchatov, Kazakhstan, e-mail: bakayeva@nnc.kz).

Gainiya K. Zhanbolatova – PhD, Senior Researcher at the National Nuclear Center of the Republic of Kazakhstan (Kurchatov, Kazakhstan, e-mail: kaiyrdy@nnc.kz).

Kadu Pramod – M.Sc., M.Phil., PhD, Postdoctoral Researcher, School of Nanoscience and Nanotechnology, Mahatma Gandhi University (Kottayam, India, e-mail: pramd.k145@gmail.com, pramodk@mgu.ac.in).

Ahmed Shakeel – PhD, Assistant Professor at the Postgraduate Department of Chemistry, Government Postgraduate College Rajouri, Higher Education Department, Government of Jammu and Kashmir (Jammu & Kashmir, India, e-mail: editorshakeel@gmail.com).